Environment. Technology. Resources. Rezekne, Latvia
Proceedings of the 14th International Scientific and Practical Conference. Volume 3, 257-261

Practice Oriented Heat Source Model Calibration

Manahil Tongov
Department of Material Sscience and Technology
Technical University of Sofia
Sofia, Bulgaria
Center of welding
(IMSETCHA) "Acad. A. Balevski" Bulgarian Academy of Sciences
Sofia, Bulgaria
tongov@tu-sofia.bg

Valentin Anguelov
Center of welding
Institute of Metal Science, Equipment and Technologies with with Center for Hydro- and Aerodynamics (IMSETCHA) "Acad. A. Balevski" Bulgarian Academy of Sciences
Sofia, Bulgaria
valentin.anguelov@ims.bas.bg

Abstract. **The modelling of the thermal process is used as a tool in determination of the properties of the materials, subject to welding. One of the most important steps in the modelling is the calibration of the heat source model. This is a necessary condition for a given model to be used to solve practical problems. The standard practice in this regard is to calibrate the model by the shape of the melted zone or by the temperature cycles at set points. In the present work, the heat source model calibration based on the maximum temperatures measured at several surface points, at different distances from the seam line, is considered. The temperature cycles in the welded joint and the penetration depth were assumed by the model, calibrated in such non-destructive way. The calculated temperature cycles were compared with records of the temperature during welding. The actual penetration depth was measured by metallographic examination of samples and compared with the assumed penetration depth. The obtained results make it possible to evaluate the suitability of the proposed methodology for determining the cooling rate in the heat affected zone.**

Keywords: heat source calibration, thermal cycles, welding.

I. INTRODUCTION

For the practical use of the various welding thermal processes models is necessary to calibrate, validate and verify them. The calibration of the model is realized by determination of parameters involved in the definition of the heat source, by comparing experimental and computational results. From this point of view, it is important that the process can be carried out through simple and quickly realizable experiments. In this study, it is proposed to use the maximum temperatures measured on the surface of the welded parts as such. Measuring of these temperatures is done in proximity to the weld seam. In addition to the maximum temperatures, it is necessary to measure the distance from the seam line to the temperature measurement point. It is obvious that one of the isotherm lines, with temperature of the solidus, is located at the seam edge. The distance to the axis of the seam is equal to half of its width.

The main types of heat source models describing the interaction of the welding arc and the article are volumetric [1] ÷ [12], surface [13] ÷ [21] or a combination of both types [22] ÷ [25]. From the volumetric heat sources the Goldak's model is most often used:

$$q = \begin{cases} \dfrac{6\sqrt{3}\eta UIf_f}{\pi\sqrt{\pi}a_f bc}\exp\left(-3\left(\dfrac{x^2}{a_f^2}+\dfrac{y^2}{b^2}+\dfrac{z^2}{c^2}\right)\right) \\ \dfrac{6\sqrt{3}\eta UIf_r}{\pi\sqrt{\pi}a_r bc}\exp\left(-3\left(\dfrac{x^2}{a_r^2}+\dfrac{y^2}{b^2}+\dfrac{z^2}{c^2}\right)\right) \end{cases} \quad (1)$$

Here U is the welding voltage, I – arc current and η – efficiency. Since $f_f = a_f/(a_f + a_r)$ and $f_r = a_r/(a_f + a_r)$ it has 4 parameters that can be used for calibration – a_f, a_r, b. and c.

Both volumetric and surface heat sources are defined in a movable coordinate system related to the welding arc. Surface heat sources are based on a Gaussian distribution

Print ISSN 1691-5402
Online ISSN 2256-070X
https://doi.org/10.17770/etr2023vol3.7206

$$q(r) = \frac{\eta UI}{2\pi R_N^2} \exp\left(-\frac{r^2}{2R_N^2}\right) \quad (2)$$

II. MATERIALS AND METHODS

In this study, the experiments were conducted by TIG welding. The process parameters are: welding current 180 A; arc voltage – 12.6 V; welding speed – 10 cm/min. The sample for conducting the experiment is made of steel S355JR with dimensions 6x240x250 mm. During the implementation of the process, temperature cycles were recorded at two points located at different distances from the seam line (Fig.1). The distance from the first point to the seam line is 7.7mm, and from the second - 9.7 mm. From these records the maximum temperatures at these points were determined to be 1000˚C and 836˚C respectively. The measured width of the weld bead is 8.5mm. In this way, the distance from the seam line to the point where the temperature reaches the solidus temperature is 4.25mm.

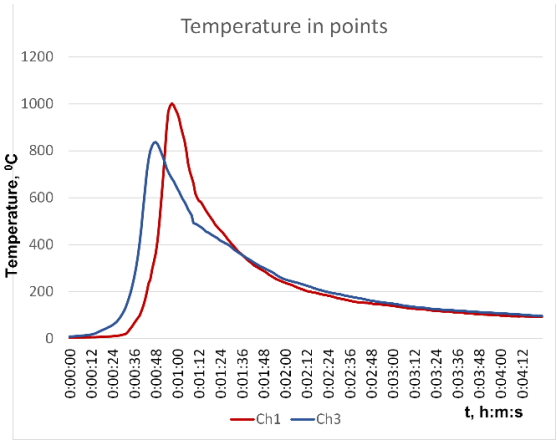

Fig. 1. Temperature records.

To solve the heat problem, the heat source described in [20] was used. The calibration was performed according to the methodology described there. The heat flux density is defined in the moving coordinate system as

$$q(r) = \eta UIAf(r) \quad (3)$$

where:

$$A = \frac{1}{\sigma\sqrt{2\pi}\exp\left(-\frac{r_0^2}{2\sigma^2}\right) + \pi r_0 erf\left(\frac{r_0}{\sigma\sqrt{2}}\right)}$$

$$f(r) = \frac{1}{2\sigma\sqrt{2\pi}}\left[\exp\left(-\frac{(r-r_0)^2}{2\sigma^2}\right) + \exp\left(-\frac{(r+r_0)^2}{2\sigma^2}\right)\right]$$

This model uses the efficiency η, effective heating radius r_{arc} and distribution coefficient $\alpha_{arc} = r_0 / r_{arc}$ as calibrating parameters. These parameters determine the values $r_0 = \alpha_{arc} . r_{arc}$ and $\sigma = r_{arc} / 3$. Minimization of the maximum relative error was used to determine the values of the calibration parameters. In the **Table I** shows the last stage of solving the optimization problem, and Fig. 2 shows the result of the calibration process.

TABLE I. FINAL STEPS OF THE CALIBRATION PROCESS.

η	r_{arc}, mm	α_{arc}	**Objective**
0.7000	9.540	0.3300	0.001036
0.7030	9.540	0.3300	0.001276
0.7000	9.510	0.3300	0.0011167
0.7000	9.540	0.3420	7.35E-04
0.6970	9.520	0.3380	9.87E-04
0.6985	9.525	0.3360	8.92E-04
0.7000	9.540	0.3360	8.81E-04
0.7000	9.525	0.3360	8.44E-04
0.7015	9.540	0.3360	9.84E-04
0.6985	9.530	0.3400	8.36E-04
0.6993	9.533	0.3390	9.02E-04
0.7000	9.533	0.3390	7.52E-04
0.7000	9.540	0.3390	8.07E-04
0.7008	9.540	0.3390	8.55E-04
0.6993	9.535	0.3410	8.55E-04
0.6996	9.536	0.3405	7.53E-04
0.7003	9.544	0.3415	7.39E-04
0.6998	9.543	0.3422	7.16E-04
0.6995	9.544	0.3430	7.88E-04
0.7000	9.544	0.3433	7.06E-04
0.7000	9.546	0.3447	7.20E-04
0.6996	9.541	0.3435	7.25E-04
0.6998	9.542	0.3430	7.27E-04
0.6999	9.543	0.3427	7.67E-04
0.7000	9.542	0.3426	7.92E-04
0.7001	9.544	0.3424	7.36E-04
0.7000	9.546	0.3430	7.05E-04
0.7001	9.547	0.3431	7.28E-04
0.7002	9.546	0.3430	7.68E-04
0.7000	9.544	0.3428	7.56E-04
0.7002	9.545	0.3430	7.98E-04
0.7000	9.544	0.3428	7.06E-04
0.6999	9.545	0.3437	7.48E-04
0.7001	9.544	0.3427	7.46E-04
0.7000	9.545	0.3431	7.02E-04
0.7000	9.545	0.3429	7.24E-04
0.7001	9.545	0.3427	7.05E-04
0.7001	9.545	0.3429	7.37E-04
0.7000	9.545	0.3429	7.26E-04
0.7001	9.545	0.3429	7.78E-04
0.7000	9.545	0.3430	7.63E-04
0.7000	9.545	0.3430	6.99E-04

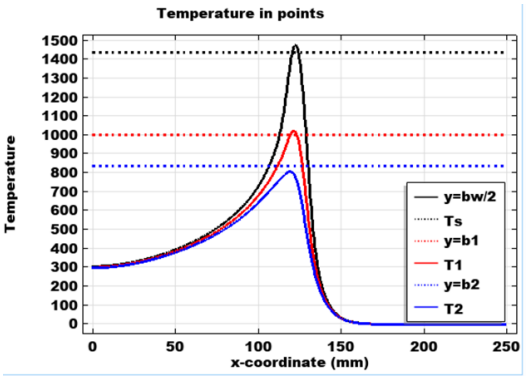

Fig. 2. Calibration result.

III. RESULTS AND DISCUSSIONS

The general view of the temperature field is presented in Fig.3 and Fig.4. Fig. 5 shows the high temperature region with isothermal surfaces plotted for the calibration values and temperatures 800˚C and 500˚C. Except for the isothermal surface for the solidus temperature, the others have an almost cylindrical shape.

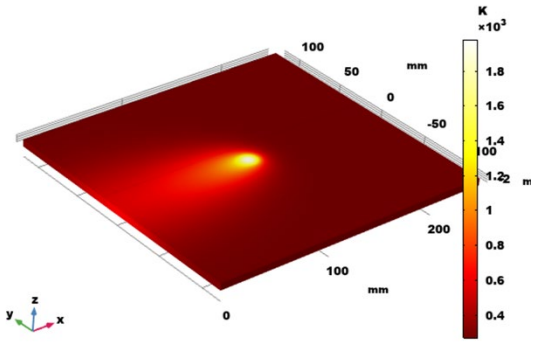

Fig. 3. Common view of temperature.

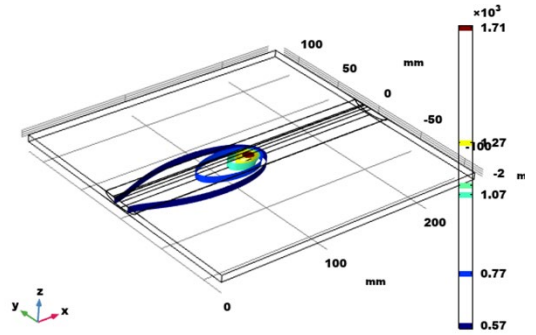

Fig. 4. Isothermal surfaces (K).

Fig. 6 shows the isothermal contours for the calibration temperatures and the liquidus temperature. It can be noted that the two-phase region is extremely small in size. Furthermore, it is also evident here that the measured temperatures have been reached at the control points. From what is shown in this figure, it follows that the deviation in the width of the 1000˚C isotherm is within 0.3 mm.

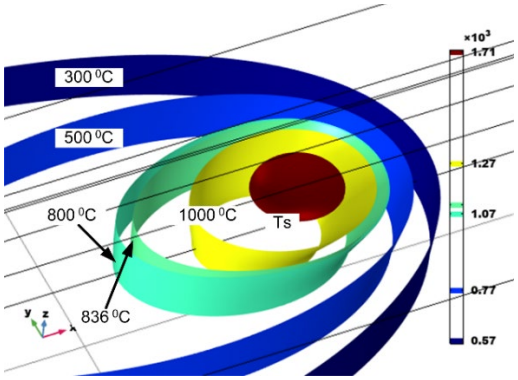

Fig. 5. Isothermal surfaces in the high temperature region.

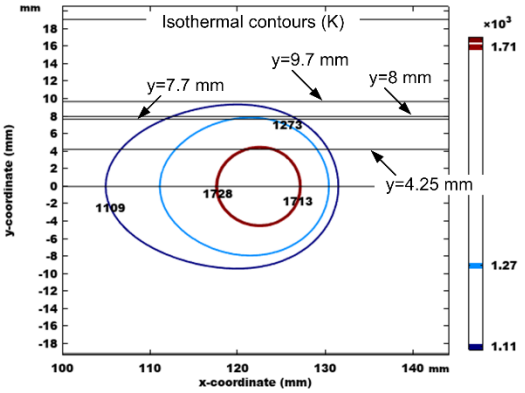

Fig. 6. Isothermal contours on top surface for calibrated distances and liquidus temperature.

One of the most important characteristics that should be determined when welding steels prone to the formation of cold cracks is the cooling time from 800˚C to 500˚C. Fig. 7 shows the isotherms at these temperatures. The seam line distance between these isotherms in the cooling zone is 30.5 mm. Since the welding speed is 10 cm/min, this means that the cooling time from 800˚C to 500˚C $t_{8/5}$ for the points of the seam line is 18.3 s.

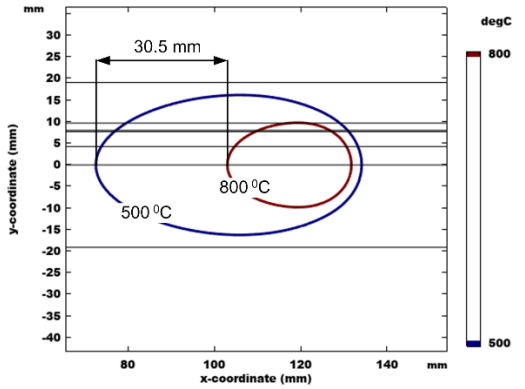

Fig. 7. Isothermal contours for $t_{8/5}$ determinating.

Table II shows experimental and calculated data on the cooling time at the control point reaching the maximum temperature of 1000˚C. The obtained experimental data indicate that the $t_{8/5}$ is 15 s. The result calculated by the model is 19.5 s. This shows that at the used cooling conditions (coefficient of convective heat removal $h = 8$ W/(m²K) and emissivity $\varepsilon = 0.4$) the measured values are lower than the calculated ones. Fig. 8 illustrates the influence of the distance from the axis of the seam on the duration of $t_{8/5}$. It can be seen that the cooling time from 800˚C to 500˚C is the least along the seam line.

TABLE II. EXPERIMENTAL AND CALCULATED DATA FOR COOLING RATE DETERMINING

Experimental			
t, h:m:s	***T, ˚C***	***t, h:m:s***	***T, ˚C***
0:01:05	800.11	0:01:13	582.84
0:01:06	746.98	0:01:14	571.02
0:01:07	712.31	0:01:15	557.55
0:01:08	687.43	0:01:16	544.28
0:01:09	662.2	0:01:17	532.52

0:01:10	619.55	0:01:18	522.28
0:01:11	600.69	0:01:19	511.00
0:01:12	586.87	0:01:20	500.32
Calculated			
t, s	***T, ˚C***	***t, s***	***T, ˚C***
44.25	816.37	54.75	608.18
45.00	796.65	55.50	597.67
45.75	777.59	56.25	587.56
46.50	759.67	57.00	577.84
47.25	742.57	57.75	568.50
48.00	726.22	58.50	559.48
48.75	710.66	59.25	550.80
49.50	695.75	60.00	542.41
50.25	681.56	60.75	534.30
51.00	667.95	61.50	526.47
51.75	654.94	62.25	518.87
52.50	642.50	63.00	511.52
53.25	630.56	63.75	504.39
54.00	619.16	64.50	497.47

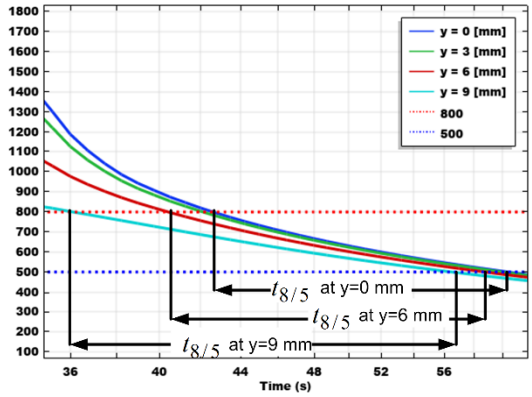

Fig. 8. Cooling time for diferend distance from seam line.

IV. CONCLUTIONS

Comparing experimental and simulation modelling results shows that the heat source model can be successfully calibrated to the maximum temperatures measured near the seam. When using constant values of the characteristics describing the convective and radiative heat removal, the obtained calculated values for the cooling time from 800˚C to 500˚C are higher than the experimentally determined ones. This means that it is important to use temperature-dependent coefficients describing the cooling process. Comparing the calculated results for points at different distances from the seam shows that, in the considered case, the lowest value of $t_{8/5}$ was obtained along the seam line.

V. ACKNOWLEDGMENTS

The authors are grateful to the financial support of the Bulgarian National Science Fund, Contract No KP-06-H57/10, for carrying out the necessary research.

REFERENCES

[1] M. A. Malik, M. E. Qureshi and N. U. Dar, Numerical Simulation of Arc Welding Investigation of various Process and Heat Source Parameters, MED UET Taxila, 2007, pp 127÷142

[2] P. B. Guimarães et all, OBTAINING TEMPERATURE FIELDS AS A FUNCTION OF EFFICIENCY IN TIG WELDING BY NUMERICAL MODELING, 21st Brazilian Congress of Mechanical Engineering October 24-28, 2011, Natal, RN, Brazil, Proceedings of COBEM, 2011, DOI: http://dx.doi.org/10.5380/reterm.v10i1-2.61952

[3] D. B. Darmadi, Validating the accuracy of heat source model via temperature histories and temperature field in bead-on-plate welding, International Journal of Engineering & Technology, October 2011, IJENS Vol: 11 No: 05

[4] J. Da Nobrega, D. Silva, B. Arauho, R. De Melo, T. Maciel, A. Silva and N. Dos Santos, Numerical evaluation of multipass welding temperature field in API 5L X80 steel welded joints. *International Journal of Multiphysics,* vol. 8, Issue 3, 2014, pp. 337-348.

[5] R. Pamnani, M. Vasudevan, T. Jayakumar, P. Vasantharaja, and K. C. Ganesh. Numerical simulation and experimental validation of arc welding of DMR-249A steel. *Defence Technology,* Vol. 12, Issue 4, August 2016, Pages 305-315, 2016, https://doi.org/10.1016/j.dt.2016.01.012

[6] W. Piekarska and K. Rek, Numerical analysis and experimental research on deformation of flat made of TIG welded 0H18N9 steel. Paper presented at the *Procedia Engineering, vol. 177, pp.* 182-187, 2017. doi:10.1016/j.proeng.2017.02.217

[7] Li, C. Chen, D. Zhao and C. Wu, Determination and Application of Double Ellipsoid Heat Source Model, International Conference on Material Science, Energy and Environmental Engineering (MSEEE 2017), Advances in Engineering Research, volume 125, pp. 267÷270, https://doi.org/10.2991/mseee-17.2017.49

[8] C.Yan, H. Jiang, L. Wu, C. Kan and W. Yu, Numerical simulation of temperature field in multiple-wire submerged arc welding of X80 pipeline steel, *IOP Conference Series: Earth and Environmental Science* vol. *108 art. No 022048,* 2018, doi:10.1088/1755-1315/108/2/022048

[9] P. Ferro, F. Berto, F. Bonollo and R.Montanari, Experimental and numerical analysis of TIG-dressing applied to a steel weldment, Procedia Structural Integrity Volume 9, pp. 64-70, 2018, https://doi.org/10.1016/j.prostr.2018.06.012

[10] H.Huang, X.Yin, Z.Feng and N.Ma, Finite element analysis and in-situ measurement of out-of-plane distortion in thin plate TIG welding. *Materials, vol. 12, Issure* 1, 2019 doi:10.3390/ma12010141

[11] M. Matuszewski, Modeling of 3D temperature field in butt welded joint of 6060 alloy sheets using the ANSYS program. Paper presented at the *IOP Conference Series: Materials Science and Engineering, vol. 659 Issure* 1, 2019 doi:10.1088/1757-899X/659/1/012034

[12] S.Zuo, Z. Wang, D. Wang, B. Du, P. Cheng, Y. Yang, P. Zhang and N. Lang, Numerical simulation and experimental research on temperature distribution of fillet welds. *Materials* ***2020****, vol. 13 Issure 5, art, No 1222; https://doi.org/10.3390/ma13051222*

[13] H. Pengfei, L. Yan, L. Yangyang and L. Zhenyang, Numerical simulation of the temperaturbe filed in fixed-TIG welding pool, 2011 International Conference on Modeling, Simulation and Control, IPCSIT vol.10 (2011) © (2011) IACSIT Press, Singapore

[14] S. Yamane, T. Yamazaki, T. Kaneta, T. Nakajima and H. Yamamoto, Experiment and numerical simulation in temperature distribution and welding distortion in GMA welding. *Yosetsu Gakkai Ronbunshu/Quarterly Journal of the Japan Welding Society, vol.* **29** Issure 3, pp. 31s-34s., 2011, https://doi.org/10.2207/qjjws.29.31s

[15] P. R. De Freitas Teixeira, D. B. De Araújo and L. A. B. Da Cunha, Study of the gaussian distribution heat source model applied to numerical thermal simulations of tig welding processes. Ciencia y Engenharia/ Science and Engineering Journal, vol. 23, Issure 1, pp. 115-122, 2014,. doi:10.14393/19834071.2014.26140

[16] H. Liu and L. Niu, Finite element simulation research on medium plate multi-pass welding temperature field. The Open Mechanical Engineering Journal, Volume 9, pp.786-790, 2015

[17] M. B. Bjelić, K. Kovanda, L. Kolarik, M. N. Vukićević and B. S. Radičević, Numerical modeling of two-dimensional heat-transfer and temperature-based calibration using simulated annealing optimization method: Application to gas metal arc welding.

Thermal Science, vol, **20,** Issure 2, pp. 655-665, 2016, doi:10.2298/TSCI150415127B

[18] M.Zhang, Y.Zhou, C. Huang, Q.Chu, W.Zhang, and J. Li Simulation of temperature distribution and microstructure evolution in the molten pool of GTAW Ti-6Al-4V alloy. Materials vol. 11, art. No 2288, 2018; https://doi.org/10.3390/ma11112288

[19] J. Wróbel and A. Kulawik Prediction of the superficial heat source parameters for TIG heating process using FEM and ANN modeling. *Entropy, vol. 21, Issure* 10, art. No 954, 2019, doi:10.3390/e21100954

[20] M. Tongov Heat Source for TIG Welding Modelling, Environment. Technology. Resources. Rezekne, Latvia, Proceedings of the 13th International Scientific and Practical Conference. Volume 3, pp. 348-356, 2021.

[21] M. TongovInvestigation of GMAW by Simulation Modelling, Environment. Technology. Resources. Rezekne, Latvia, Proceedings of the 13th International Scientific and Practical Conference. Volume 3, pp. 357-362, 2021.

[22] A.Moarrefzadeh and M.A.Sadeghi, Numerical Simulation of Thermal Profile By Gas Tungsten Arc Welding Process in Copper, Wseas transactions on heat and mass transfer, Volume 5, Issue 3, July 2010, ISSN: 1790-504

[23] Y. Saadlaoui, E. Feulvarch, A. Delache, J. Leblond and J. Bergheau, A new strategy for the numerical modeling of a weld pool. *Comptes Rendus - Mecanique,* Vol. 346, Issue 11, pages 999-1017, November 2018, https://doi.org/10.1016/j.crme.2018.08.007.

[24] T.F. Flint and M.C.Smith, HEDSATS: High energy density semi-analytical thermal solutions. *SoftwareX,* Volume 10, art. No 100243, July–December 2019, https://doi.org/10.1016/j.softx.2019.100243

[25] K. Agrebi, A. Belhadj and M. Bouhafs, THREE-DIMENSIONAL NUMERICAL SIMULATION OF A GAS TUNGSTEN ARC WELDING PROCESS, IJTech International Journal of Technology, vol. 10 Issure 4, pp. 689-699, 2019, ISSN 2086-9614, DOI: https://dx.doi.org/10.14716/ijtech.v10i4.1849